Draft version November 4, 2025
Typeset using LaTeX **twocolumn** style in AASTeX7

Limits on forming coreless terrestrial worlds in the TRAPPIST-1 system

Dongyang Huang [1,2] and Caroline Dorn [3]

[1] SKLab-DeepMinE, MOEKLab-OBCE, School of Earth and Space Sciences, Peking University, 100871 Beijing, China
[2] Research Institute of Extraterrestrial Material at PKU (RIEMPKU)
[3] Institute for Particle Physics and Astrophysics, ETH Zürich, 8093 Zürich, Switzerland

ABSTRACT

With seven temperate Earth-sized planets revolving around an ultracool red dwarf, the nearby TRAPPIST-1 system offers a unique opportunity to verify models of exoplanet composition, differentiation, and interior structure. In particular, the low bulk densities of the TRAPPIST-1 planets, compared to terrestrial planets in our solar system, require either substantial amount of volatiles to be present or a corefree scenario where the metallic core is fully oxidised. Here, using an updated metal–silicate partitioning model, we show that during core–mantle differentiation oxygen becomes more siderophile (iron-loving) implying larger planet radii. For the seven TRAPPIST-1 planets, however, we find that they are not sufficiently large to oxidise all the iron in the core, if they differentiate from an Earth-like composition. Oxygen partitioning in rocky worlds precludes coreless planets up to $\sim$4 $M_\oplus$. The observed density deficit in the TRAPPIST-1 planets, and more generally in M dwarf systems if confirmed by future observations, may be explained by system-dependent element budgets during planet formation, which are intrinsically linked to their stellar metallicity.

Keywords: Exoplanets (498) — Exoplanet structure (495) — Exoplanet formation (492)

1. INTRODUCTION

TRAPPIST-1 is a low-mass ($\sim$0.09 $M_\odot$) M8 dwarf star, at a distance of $\sim$12 parsecs from Earth, with seven Earth-sized transiting rocky planets located within or near the edge of its habitable zone (M. Gillon et al. 2017). As an important target for both detecting the atmospheric signatures of potentially habitable worlds and for testing theories of formation, migration, and interior structure for terrestrial planets around M dwarfs, the system has received much attention since its discovery (R. Luger et al. 2017; B. Quarles et al. 2017; S. L. Grimm et al. 2018; E. Agol et al. 2021; J. Krissansen-Totton & J. J. Fortney 2022; C. Piaulet-Ghorayeb et al. 2025). In particular, based on transit photometry and transit-timing variations (TTVs), the planetary radii and masses are constrained to $\sim$0.76–1.1 $R_\oplus$ and $\sim$0.3–1.4 $M_\oplus$, both to a precision of less than 5% (S. L. Grimm et al. 2018; E. Agol et al. 2021), establishing the Earth-like nature in all seven planets. All seven TRAPPIST-1 planets follow an iso-chemical trend in the mass–radius diagram (E. Agol et al. 2021) with densities slightly lower than an Earth-like composition; we refer to this as the 'density deficit'. Like compositional models designed to account for the mass–radius relationships for exoplanets (S. Seager et al. 2007; C. Dorn et al. 2015; L. Zeng et al. 2019; L. Noack & M. Lasbleis 2020; R. Luque & E. Pallé 2022; R. J. Spaargaren et al. 2023), the interpretation of the nature of this density deficit suffers from the degeneracy between rocky components (including an iron core, a silicate mantle) and volatile-rich components (C. T. Unterborn et al. 2018a; E. Agol et al. 2021). For instance, the estimated amount of water, the most popular volatile species, from varying models ranges from dry, or Earth-like (0.001–5 wt%) (C. Dorn et al. 2018a; E. Agol et al. 2021) to water-rich worlds (15–$\geq$50 wt%) (B. Quarles et al. 2017; C. Dorn et al. 2018a; C. T. Unterborn et al. 2018a) for the TRAPPIST-1 planets.

Alternative solutions to the density deficit include varying core–mantle fraction (CMF) or Fe/Mg ratio (D. Valencia et al. 2007; E. Agol et al. 2021), or an extreme core-free scenario where all the iron in the core is oxidised and mixed with the mantle (L. T. Elkins-Tanton & S. Seager 2008; E. Agol et al. 2021).

From a planet formation perspective, it is possible that the TRAPPIST-1 planets formed beyond the snow line and migrated inward (e.g. D. Schoonenberg et al.

Email: dhuang@pku.edu.cn, dornc@phys.ethz.ch

2019), implying that significant amounts of water are possible. However, H. Chen et al. (2025) argued that rocky planets in compact M-dwarf systems form depleted in volatiles, allowing for only few Earth oceans accreted from the TRAPPIST-1 planets. The sustainability of atmospheres or the presence of surface oceans is thus limited. This is also supported by the fact that any atmosphere may be subject to efficient loss leaving behind negligibly thin atmospheres (G. Van Looveren et al. 2025; E. K. Pass et al. 2025) with no effect on mass-radius relationships.

Recent JWST observations of the TRAPPIST-1 system indicate that the two innermost planets, TRAPPIST-1 b and c, lack substantial atmospheres (J. Ih et al. 2023; T. P. Greene et al. 2023; O. Lim et al. 2023; A. P. Lincowski et al. 2023; S. Zieba et al. 2023; E. Ducrot et al. 2025; M. Radica et al. 2025): their thermal phase curves show poor heat redistribution, and transmission spectra are featureless, consistent with bare-rock surfaces. This aligns with theoretical expectations that intense stellar irradiation (4.2 $\times$ and 2.2 $\times$ Earth's insolation, respectively) would have driven atmospheric loss via hydrodynamic escape. TRAPPIST-1 d, receiving more moderate flux, remains a marginal case—models suggest roughly a 70% probability of retaining some atmosphere (J. Krissansen-Totton 2023; M. T. Gialluca et al. 2024), though others are less optimistic (G. Van Looveren et al. 2025). JWST observations rule out clear hydrogen-rich or dense CO_2- and CH_4-rich atmospheres ($> 3\sigma$ confidence), instead favoring either an extremely tenuous or aerosol-laden atmosphere, or none at all (C. Piaulet-Ghorayeb et al. 2025). Previous Hubble and Spitzer data were only sensitive enough to exclude clear, low–mean-molecular-weight atmospheres, leaving high–mean-molecular-weight or hazy compositions unconstrained. Overall, spectroscopic observations are consistent with the absence of any thick atmospheres on the innermost three planets.

The absence of a thick atmosphere reduces the degeneracy in possible interior models to the composition and layer thicknesses of a core and a mantle. Interior structure models often rely on first-order assumptions. Commonly, planets are modeled as a set of separate layers of distinct compositions or phases. This limitation, among other factors, adds to the degeneracy of interior models and limits their accuracy. The reason is that commonly used interior models neglect core–mantle partitioning of volatiles (such as H, C and N) which is prevalent during planet formation (Y. Li et al. 2020; R. A. Fischer et al. 2020; D. Huang et al. 2024). A recent work calculated global water distribution between exoplanet cores and mantles using a thermodynamic integration method (H. Luo et al. 2024). The majority of the accreted water of a planet is found to be stored deep in the metal core, reducing the available surface water by orders of magnitudes. This finding was confirmed by chemical equilibration models to be valid also for sub-Neptunes (A. Werlen et al. 2025). Water is efficiently lost to the deep interior. Volatile partitioning in deep interiors is essential for accurate models, as surface reservoirs alone can differ by orders of magnitude from the total bulk inventory (e.g. C. Dorn & T. Lichtenberg 2021; H. Luo et al. 2024). Bulk volatile abundances are what link a planet to its primordial composition, providing the key to reconstructing its formation pathway and original location within the protoplanetary disk, as is the case with the provenance of the terrestrial C, N and S budgets (D. Huang et al. 2024).

For modeling the interiors of the TRAPPIST-1 planets, we are agnostic about the volatile-rich terrestrial planets, as the partitioning behaviour of most volatile species remains undetermined at pressures (100–1000 GPa) and concentration level (> 10 wt%) relevant to exoplanet interiors. Furthermore, we test different assumptions for planetary core–mantle fraction (CMF). We use the canonical assumption that the TRAPPIST-1 planets follow an Earth-like CMF; and also test a CMF that is based on TRAPPIST-1 stellar metallicity estimates (M. Gillon et al. 2016) and its interpretation regarding bulk Fe/Mg (C. T. Unterborn et al. 2018b). Here we propose to explore the third scenario, i.e. the coreless case, by devising a thermodynamic model for the partitioning of oxygen between cores and mantles of Earth-sized exoplanets. After testing the viability of the coreless scenario in the TRAPPIST-1 system, which provides a rare statistics with seven terrestrial planets within a single system, we extend our discussions to potential implications for atmospheric signatures as a consequence of core–mantle–atmosphere equilibration.

2. METHODS

2.1. *Thermodynamic model: oxygen partitioning between the core and mantle of rocky planets*

Oxygen (O) is the third most abundant element in the solar system after H and He (K. Lodders 2003), and the most abundant element, apart from Fe, in Earth (H. S. Wang et al. 2018). Consequently, the partitioning of O between Fe metal and silicate determines the extent to which the metallic core is oxidised.

Oxygen partitioning to iron was previously considered limited based on experiments performed at relatively low pressures up to Earth's upper mantle conditions. Thanks to recent advances in laser-heated diamond anvil cell experiments (e.g. M. A. Bouhifd & A. P. Jephcoat

2011; J. Siebert et al. 2012), numerous new data became available in the past decade, where O was found to dissolve into Fe in substantial amounts at Earth's core–mantle boundary pressure (J. Siebert et al. 2013; J. Badro et al. 2016; D. Huang & J. Badro 2018; D. Huang et al. 2020, 2021, 2024). This makes it possible to device a new thermodynamic model for oxygen. The partitioning of O is accompanied by the dissolution of oxides from the silicate into the metal, which, in terms of major rock-forming cations (Si, Mg, and Fe), can be described by

$$SiO_2^{silicate} \rightleftharpoons Si^{metal} + 2O^{metal}, \tag{1}$$

$$MgO^{silicate} \rightleftharpoons Mg^{metal} + O^{metal}, \tag{2}$$

and

$$FeO^{silicate} \rightleftharpoons Fe^{metal} + O^{metal}, \tag{3}$$

whose universal form is therefore

$$[O^{2-}]^{silicate} \rightleftharpoons [O^0]^{metal}. \tag{4}$$

The equilibrium constant K of reaction 4, defined in terms of activities (a_i) of the components, their mole fractions c_i and activity coefficients γ_i in relevant phases, is given by

$$K = \frac{a_{O^0}^{metal}}{a_{O^{2-}}^{silicate}} = \frac{c_{O^0}^{metal} \cdot \gamma_{O^0}^{metal}}{c_{O^{2-}}^{silicate} \cdot \gamma_{O^{2-}}^{silicate}}. \tag{5}$$

Assuming only temperature dependence for $\gamma_{O^0}^{metal}$, the term can be approximated as the activity of O in liquid Fe in infinite dilution, of which we take the form provided by J. Badro et al. (2015). $\gamma_{O^{2-}}^{silicate}$ is unknown, and is assumed to be unity, as O is by number the most abundant species in the silicate. For experimentally determined concentrations of oxygen (c_i in metal and silicate phases), we use the compilation by D. Huang et al. (2024). Their ratio is by definition the partition coefficient D of oxygen between metal and silicate

$$D_O = c_{O^0}^{metal} / c_{O^{2-}}^{silicate}. \tag{6}$$

Based on thermodynamic relations, equilibrium constant K can be expressed as a function of P (in GPa) and T (in K) (D. Huang et al. 2021, 2024); by fitting the experimental data and by rearranging Eqs. 5–6, one obtains

$$D_O = \frac{10^{2.066(\pm 0.280) - 12378(\pm 697)/T + 37.76(\pm 8.97) \cdot P/T}}{exp(4.29 - 16500/T)}. \tag{7}$$

2.2. *Interior models coupled with oxygen partitioning*

In order to quantify the implications of self-consistent oxygen partitioning for planet interiors, we build upon the models from (C. Dorn et al. 2015, 2017) with latest updates in (H. Luo et al. 2024). For this application, the planets of interest are rocky worlds only.

We consider a core made of Fe, and FeO. For solid Fe, we use the equations of state for hexagonal close packed (hcp) iron (K. Hakim et al. 2018; F. Miozzi et al. 2020). For liquid iron, we use H. Luo et al. (2024). The core thermal profile is assumed to be adiabatic throughout the core. At the core-mantle boundary (CMB), there is a temperature jump as the core can be hotter than the mantle due to the residual heat released during core formation. We follow L. Stixrude (2014) and add a temperature jump at the CMB temperature such that the temperature at the top of the core is at least as high as the melting temperature of the silicates.

The amount of FeO in the core is calculated from the partitioning coefficient of oxygen following equation 6. As the mass fraction of FeO can vary between 0 and 1, corresponding oxygen mass fraction ranges between zero and 0.22. For the equilibration, we use a pressure that equals 30% of the pressure at the core-mantle-boundary (CMB) and a temperature equal to the dry melting temperature of silicates at this corresponding pressure plus 1000 K.

The mantle is assumed to be composed of three major constituents, i.e., MgO, SiO_2, FeO. For the solid mantle, we use the thermodynamical model `Perple_X` J. Connolly (2009), to compute stable mineralogy and density for a given composition, pressure, and temperature, employing the database of L. Stixrude & C. Lithgow-Bertelloni (2022). For pressures higher than ~ 125 GPa, we define stable minerals *a priori* and use their respective equation of states from various sources (R. A. Fischer et al. 2011; S. Faik et al. 2018; Y. Luo et al. 2023; R. J. Hemley et al. 1992; R. Musella et al. 2019). For the liquid mantle, we calculate its density assuming an ideal mixture of main components (Mg_2SiO_4,SiO_2,FeO) (S. T. Stewart et al. 2020; S. Faik et al. 2018; H. Melosh 2007; H. Ichikawa & T. Tsuchiya 2020) and add them using the additive volume law. Note that we use Mg_2SiO_4 melt instead of MgO melt since the data for forsterite has been recently updated for the high-pressure temperature regime, which is not available for MgO to our knowledge. The mantle is assumed to be fully adiabatic.

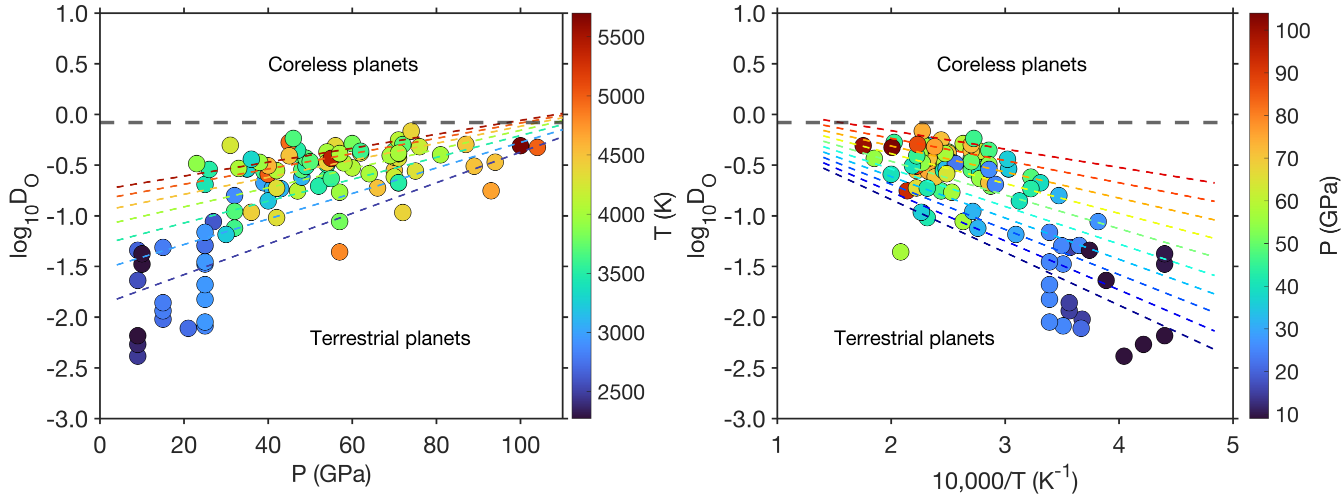

Figure 1. Core–mantle partition coefficient of oxygen as a function of pressure and temperature. Left: Experimental data for metal–silicate partitioning of O obtained at high pressures up to 104 GPa. Horizontal dashed line located at D_O=0.83 indicates full oxidation of the core (see the main text), and therefore distinguishes 'terrestrial' from 'coreless' planets. It is clear that, within the investigated pressure range, D_O asymptotically approaches the dashed line, but never reaches the core-free regime, albeit higher pressures and temperatures promote the sequestration of O into the metallic core, i.e. larger D_O. Right: The same dataset for O partitioning plotted as a function of reciprocal temperature. Dashed lines are fitted results (Eq. 7) showing the dependence of O partitioning on temperature at a given pressure or vice versa.

3. RESULTS

3.1. *Pressure and temperature dependence of O partitioning: Insights from recent LHDAC experiments*

The most remarkable feature of the O partitioning is its positive correlation to increasing pressure and temperature, which corresponds to more massive planets with deeper magma oceans during their formations. Despite of the scattering nature of the experimental data at a specific pressure, which is somewhat unavoidable as experimental results are affected by other variables, such as temperature and composition, apart from the control variable pressure (D. Huang et al. 2024), the overall positive correlation between D_O and pressure (and temperature) is evident (Fig. 1, left panel). At a given pressure, temperature increases D_O, partitioning more O into the core; at a given temperature, higher pressure similarly makes O more siderophile (Fig. 1, right panel). Because the molar fraction of O in an Earth-like mantle is invariant with $c_{O^{2-}}^{silicate} =\sim 0.6$, given a terrestrial Mg/Si molar ratio of 0.9–1.2, if the core is fully oxidised with the Fe/O molar ratio equals unity, in principle the core-free planets emerge when $D_O = 0.83$ (dashed lines in Fig. 1), as a result of sufficiently high pressure core–mantle differentiation. An equally significant observation from these experiments is that, although the partition coefficient of O points to the direction of coreless planets, as D_O asymptotically approaches 0.83, it remains within the 'terrestrial' regime with differentiated core and mantle for the pressure regime of interest.

3.2. *Oxygen content of the core increases with planet mass*

We aim to quantify implications of the new oxygen partitioning model for interior structures of super-Earths. As the partitioning coefficient of oxygen increases with higher pressure and asymptotically reaches the value of 0.83, we expect a clear dependency of core oxygen content with planet mass. Figure 2 clearly illustrates that more massive planets have more oxidized cores than smaller planets. As a result, pure iron cores become implausible for large planet masses. Instead, planets beyond $\sim$ 3.5 $M_\oplus$, are expected to have fully oxidized cores as predicted by our oxygen partitioning model. Such planets experience equilibration pressures beyond 200 GPa, where no experimental data is currently available. The experimentally constrained pressure range only reaches $\sim$ 110 GPa (Figure 2. Such pressures are relevant for silicate-metal equilibration up to planet masses of $\sim$1.6 $M_\oplus$. This is true under the assumption that the equilibration pressures are 30 % of the CMB pressure. If the overall equilibration happens deeper in planet mantles, the range of planet masses that is covered by the experimental data would be more restricted to smaller masses. In general, the trend of increasing core oxygen content with planet mass is a robust finding, the actual gradient differs upon assumptions of the equilibration pressure and temperature.

Further, our oxygen partitioning model agrees with independent estimates for Mars, Earth, and Venus, although constraints for the terrestrial planets are limited (Fig. 2). The values for the terrestrial planets come from D. Huang et al. (2023) and A. Khan et al. (2023) for Mars, R. Trønnes et al. (2019) for Venus, and K. Hirose et al. (2021) for Earth.

3.3. *M-R diagram revisited: the TRAPPIST-1 planets*

It is clear that the TRAPPIST-1 planets span a range of masses that would imply different oxygen core contents ranging from 0.01 to 0.05 wt%. Can this trend be observed or tested? Figure 3 shows mass-radius curves that incorporate self-consistently the change in core FeO content with planet mass (blue lines). First, we compare the new self-consistent interior model assuming identical solar refractory (Fe, Si, Mg) abundance: Compared to a standard rocky interior model with a pure iron and an iron-free mantle (orange dashed line), there is little difference over the small mass range of the TRAPPIST-1 planets (orange dashed line is similar to the blue solid line). Only for larger masses > 3.5 $M_\oplus$, when the metal phase are saturated with oxygen, the mass-radius curves (blue solid) will approach the densities for the core-free case (pink dotted line).

The core-free interior density for solar abundance (pink dotted) is only 5% lower from the pure Fe-core (orange dashed). Interestingly, this small density decrease is just right to fit all TRAPPIST-1 planets which was an intriguing result from E. Agol et al. (2021). Of course, there is inherent degeneracy and the TRAPPIST-1 planets can also be explained by lower Fe/Mg bulk ratios or by individual variations in water content from planet to planet. However, the latter scenario is less probable, as spectroscopic observations with JWST have ruled out thick atmospheres for the innermost planets, and reproducing the required planet-by-planet water fractions would demand finely tuned formation pathways. Here, we now add strong constraints from mineral physics to exclude the core-free scenario.

If we allow refractory element ratios to depart from solar, the mass-radius trend will differ. We adopt bulk abundance constraints as suggested by C. T. Unterborn et al. (2018a) who analyzed F-G-K stars of similar metallicity to TRAPPIST-1 and estimate a median of Fe/Si $= 1.49 \pm 0.4$ in mass ratios, while fixing the Mg/Si mass ratio to 0.87. Using a similar approach but excluding thick-disc stars, L. Acuña et al. (2021) estimated a very similar median of Fe/Si = 1.51. For comparison, the solar mass ratio estimates are Fe/Si = 1.69. With the adopted abundance from C. T. Unterborn et al. (2018a), all planets except for TRAPPIST-1 g ($T_{eq} = 199$K) fall onto the rocky mass-radius curve for equilibrated Fe-FeO (blue dash-dotted line) within their 1-σ uncertainties. Note that it is the difference in stellar abundances that allows most planets to be fitted within their 1-σ error bars, while changes due to Fe/FeO equilibration are minor across the range of TRAPPIST-1 planets.

4. DISCUSSION

Whether or not FeO cores would actually form from silicate melts early in planet histories remains an open question for planet masses > 3.5 $M_\oplus$. The current experimental constraints and thermodynamic model show the asymptotical trend of O partitioning towards a fully oxidised core (Fig. 1). This may allow for a coreless scenario (L. T. Elkins-Tanton & S. Seager 2008) at higher P-T conditions within more massive planets. To verify whether FeO can differentiate to form a core or not, new high-pressure experiments under expanded P–T–composition space would be necessary in the future (see Luo et al. in prep.). If verified, experimentally or theoretically, the predicted FeO core, existing when $M_P > 3.5$ $M_\oplus$(Fig. 2), could readily become miscible with silicate melts, potentially refuting the conventional assumption that interiors of large rocky planets have to differentiate into a layered structure.

Similarly, based on mixing properties in the binary $MgSiO_3$–Fe (in fact MgO–Fe), $MgSiO_3$–H_2, and Fe-H_2 systems, E. D. Young et al. (2025) concluded that $MgSiO_3$, Fe, and H_2 become fully miscible in deep interiors of molten cores (anything beneath the outer envelope, i.e. including silicate mantles and metallic cores) of sub-Neptunes or their super-Earth descendants. Considering the enhanced oxygen partitioning at high P-T conditions, FeO instead of pure Fe, is a more likely endmember and may enable full miscibility at even shallower depths.

The partitioning of oxygen into the metal phase has important implications for atmospheres of sub-Neptunes and super-Earths. Firstly, the oxidation of metallic iron limits the amount of O available to oxidize H. As a result, the amount of atmospheric H_2O that can be outgassed would decrease with increasing planet mass. This is broadly consistent with H. E. Schlichting & E. D. Young (2022), where water concentrations in silicate mantles and envelopes of super-Earths are significantly lower if one takes into account the chemical equilibration between the core, mantle, and atmosphere. Secondly, as noted by A. Werlen et al. (2025), parameters such as planet mass, relative mass fractions of core–mantle–atmosphere, all strongly influence the atmospheric C/O ratio. In a closed system with fixed

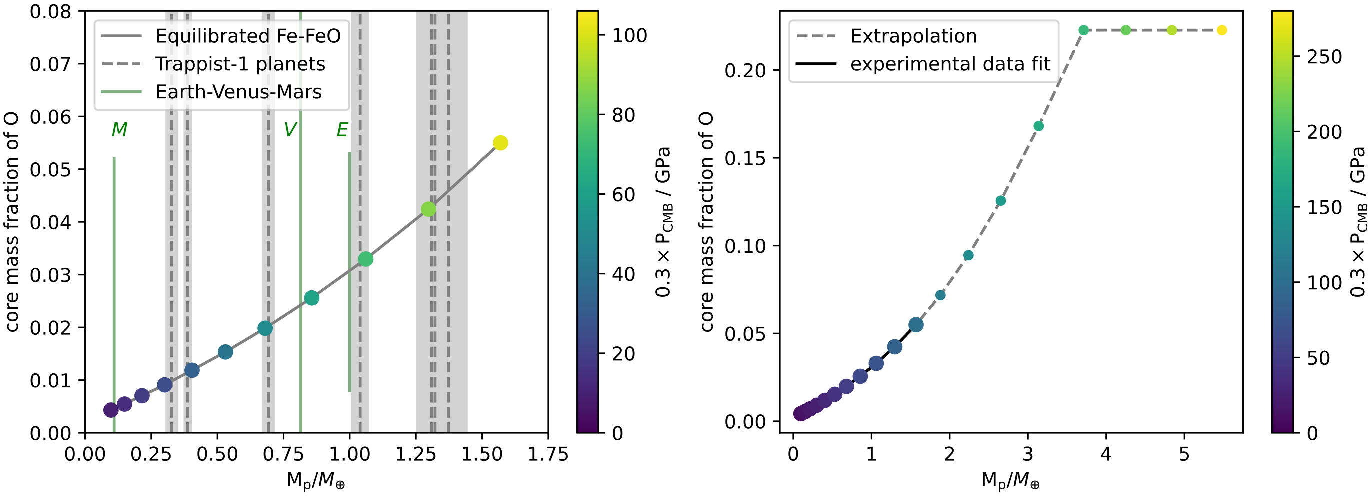

Figure 2. Equilibrated core oxygen mass fraction as a function of planetary mass. Left: Results within the pressure range constrained by experimental data. Calculated core mass fractions are compared with independent estimates for Earth and Mars, and the mass range of the TRAPPIST-1 planets is also indicated. Right: Extrapolation of the Fe–FeO equilibration model to higher masses and pressures. The oxygen mass fraction approaches an upper limit of 0.22, corresponding to complete oxidation of the core as FeO. In reality, this limit would be approached asymptotically rather than a sharp transition shown at 3.5 $M_\oplus$.

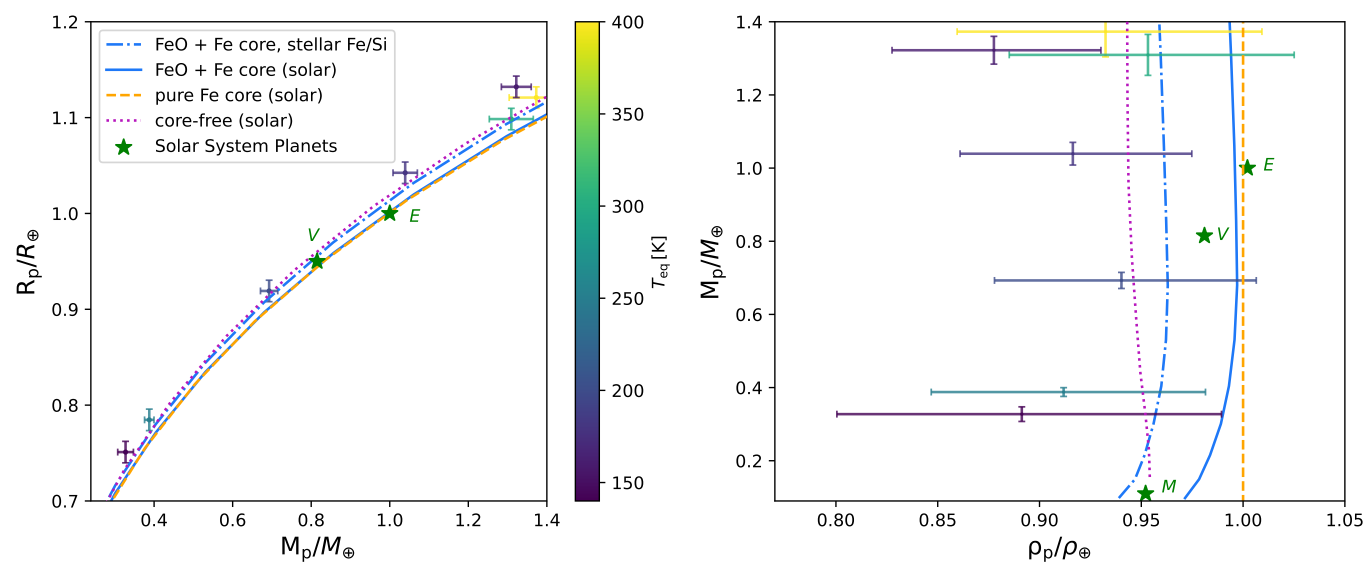

Figure 3. Left: Mass-radius diagram compared to the TRAPPIST-1 planets. Right: mass-normalized density diagram. Densities are normalized to the nominal model of a pure Fe core with solar Fe/Si abundances (orange line). The equilibrated Fe-FeO curve where oxygen partitioning is self-consistently modeled for solar Fe/Si (blue solid line) plots between the end-members of a pure Fe core (orange line) and core-free model (pink line). When the stellar Fe/Si estimate from (C. T. Unterborn et al. 2018a) is used, the equilibrated Fe-FeO line shifts to lower densities, well fitting all seven TRAPPIST planets.

initial amounts of C and O (L. Schaefer & B. Fegley 2017), if the metal–silicate (metallic core–silicate magma ocean) equilibration is considered, the partitioning of both elements into iron would determine the amounts of C and O available in the magma ocean, which would eventually modify the observed atmospheric C/O ratios owing to magma ocean-atmosphere interactions (C. Seo et al. 2024; T. Lichtenberg & Y. Miguel 2025; M. C. Nixon et al. 2025).

A caveat with the current model of O partitioning is that it is established on the basis of experimental data on relatively 'dry' terrestrial materials (D. Huang & J. Badro 2018; D. Huang et al. 2020, 2021, 2024), and is hence applicable to rocky interiors or lava planets in the regime of Henry's law; its applicability to ocean planets (M. J. Kuchner 2003; A. Léger et al. 2004), formed beyond the snow line and containing 10s wt% level of water, may be limited and requires further investigations by the mineral physics community in the future. As a step towards a more realistic scenario, future studies should address interactions among volatiles (H, C, N and O) when metal and silicate react with each other (e.g. D. Huang et al. 2024), and how they affect the partitioning and thereby atmospheric compositions.

5. CONCLUSIONS

We present a new equilibration model for Fe–FeO core phases that predicts the oxygen content of the metal phase under given pressure–temperature conditions. The model is constrained by experimental data spanning pressures from a few GPa up to 104 GPa (D. Huang et al. 2024). Our results show a clear trend of increasing oxygen incorporation with increasing planetary mass, under the assumption that equilibration pressure scales with mass. Although extrapolation is required beyond 2 $M_\oplus$, where equilibration pressures exceed experimental limits, the model predicts that pure Fe cores become impossible above a critical planet mass. Specifically, the extrapolation suggests this threshold occurs near 3.5 $M_\oplus$, though the exact value depends on the assumptions adopted here. The key result is that beyond this critical mass, the metallic core will be saturated with oxygen.

The implications for the TRAPPIST-1 planets are that coreless scenarios can be ruled out, and that the FeO content among the planets likely ranges from 0.01 to 0.05 wt%. Previously, the possible interior configurations included coreless models, variations in bulk Fe/Mg (or Fe/Si) ratios, and volatile-rich compositions. However, given recent spectroscopic observations from JWST and evolutionary constraints on water loss, we are left with a single plausible explanation: the Fe/Mg (or Fe/Si) ratios are sub-solar. This interpretation is consistent with previous estimates of the stellar composition (C. T. Unterborn et al. 2018b; C. Dorn et al. 2018b; L. Acuña et al. 2021). The fact that super-Earth metal phases become oxygen saturated for high mass planets has possible implications for any atmosphere that can degas from an early mantle magma ocean, including the observed atmospheric H_2O and C/O ratio.

ACKNOWLEDGMENTS

D.H. acknowledges supports from PKU startup grant (No. 7100604887) and the National Natural Science Foundation of China (NSFC) under grant 8206100810. C.D. gratefully acknowledges support from the Swiss National Science Foundation under grant TMSGI2_211313. This work has been carried out within the framework of the NCCR PlanetS supported by the Swiss National Science Foundation under grant 51NF40_205606.

AUTHOR CONTRIBUTIONS

All authors contributed equally to the manuscript.

REFERENCES

Acuña, L., Deleuil, M., Mousis, O., et al. 2021, Astronomy & Astrophysics, 647, A53

Agol, E., Dorn, C., Grimm, S. L., et al. 2021, Planetary Science Journal, 2, 1, doi: 10.3847/PSJ/abd022

Badro, J., Brodholt, J. P., Piet, H., Siebert, J., & Ryerson, F. J. 2015, Proceedings of the National Academy of Sciences of the United States of America, 112, 12310, doi: 10.1073/pnas.1505672112

Badro, J., Siebert, J., & Nimmo, F. 2016, Nature, 536, 326, doi: 10.1038/nature18594

Bouhifd, M. A., & Jephcoat, A. P. 2011, Earth and Planetary Science Letters, 307, 341, doi: 10.1016/j.epsl.2011.05.006

Chen, H., Clement, M. S., Wang, L., & Gu, J. T. 2025, The Astrophysical Journal Letters, 991, L11, doi: 10.3847/2041-8213/adf282

Connolly, J. 2009, Geochemistry, geophysics, geosystems, 10

Dorn, C., Khan, A., Heng, K., et al. 2015, Astronomy & Astrophysics, 577, A83, doi: 10.1051/0004-6361/201424915

Dorn, C., & Lichtenberg, T. 2021, The Astrophysical Journal Letters, 922, L4, doi: 10.3847/2041-8213/ac33af

Dorn, C., Mosegaard, K., Grimm, S. L., & Alibert, Y. 2018a, The Astrophysical Journal, 865, 20, doi: 10.3847/1538-4357/aad95d

Dorn, C., Mosegaard, K., Grimm, S. L., & Alibert, Y. 2018b, The Astrophysical Journal, 865, 20, doi: 10.3847/1538-4357/aad95d

Dorn, C., Venturini, J., Khan, A., et al. 2017, Astronomy & Astrophysics, 597, A37, doi: 10.1051/0004-6361/201628708

Ducrot, E., Lagage, P. O., Min, M., et al. 2025, Nature Astronomy, 9, 358, doi: 10.1038/s41550-024-02428-z

Elkins-Tanton, L. T., & Seager, S. 2008, The Astrophysical Journal, 688, 628, doi: 10.1086/592316

Faik, S., Tauschwitz, A., & Iosilevskiy, I. 2018, Computer Physics Communications, 227, 117, doi: 10.1016/j.cpc.2018.01.008

Fischer, R. A., Campbell, A. J., Shofner, G. A., et al. 2011, Earth and Planetary Science Letters, 304, 496, doi: 10.1016/j.epsl.2011.02.025

Fischer, R. A., Cottrell, E., Hauri, E., et al. 2020, Proceedings of the National Academy of Sciences of the United States of America, 117, 8743, doi: 10.1073/pnas.1919930117

Gialluca, M. T., Barnes, R., Meadows, V. S., et al. 2024, The Planetary Science Journal, 5, 137

Gillon, M., Jehin, E., Lederer, S. M., et al. 2016, Nature, 533, 221, doi: 10.1038/nature17448

Gillon, M., Triaud, A. H., Demory, B. O., et al. 2017, Nature, 542, 456, doi: 10.1038/nature21360

Greene, T. P., Bell, T. J., Ducrot, E., et al. 2023, Nature, 618, 39, doi: 10.1038/s41586-023-05951-7

Grimm, S. L., Demory, B.-o., Gillon, M., et al. 2018, Astronomy & Astrophysics, 613, A68, doi: 10.1051/0004-6361/201732233

Hakim, K., Rivoldini, A., Van Hoolst, T., et al. 2018, Icarus, 313, 61, doi: 10.1016/j.icarus.2018.05.005

Hemley, R. J., Stixrude, L., Fei, Y., & Mao, H. K. 1992, in High-Pressure Research: Application to Earth and Planetary Sciences (American Geophysical Union (AGU)), 183–189, doi: 10.1029/GM067p0183

Hirose, K., Wood, B., & Vočadlo, L. 2021, Nature Reviews Earth & Environment, 2, 645, doi: 10.1038/s43017-021-00203-6

Huang, D., & Badro, J. 2018, American Mineralogist, 103, 1707, doi: 10.2138/am-2018-6651

Huang, D., Badro, J., & Siebert, J. 2020, Proceedings of the National Academy of Sciences, 117, 27893, doi: 10.1073/pnas.2007982117

Huang, D., Li, Y., Khan, A., et al. 2023, Geophysical Research Letters, 50, 1, doi: 10.1029/2022GL102271

Huang, D., Siebert, J., & Badro, J. 2021, Geochimica et Cosmochimica Acta, 310, 19, doi: 10.1016/j.gca.2021.06.031

Huang, D., Siebert, J., Sossi, P., et al. 2024, Geochimica et Cosmochimica Acta, 376, 100, doi: 10.1016/j.gca.2024.05.010

Ichikawa, H., & Tsuchiya, T. 2020, Minerals, 10, 59, doi: 10.3390/min10010059

Ih, J., Kempton, E. M.-R., Whittaker, E. A., & Lessard, M. 2023, The Astrophysical Journal Letters, 952, L4, doi: 10.3847/2041-8213/ace03b

Khan, A., Huang, D., Durán, C., et al. 2023, Nature, 622, 718, doi: 10.1038/s41586-023-06586-4

Krissansen-Totton, J. 2023, The Astrophysical Journal Letters, 951, L39

Krissansen-Totton, J., & Fortney, J. J. 2022, The Astrophysical Journal, 933, 115, doi: 10.3847/1538-4357/ac69cb

Kuchner, M. J. 2003, The Astrophysical Journal, 596, L105, doi: 10.1086/378397

Li, Y., Vočadlo, L., Sun, T., & Brodholt, J. P. 2020, Nature Geoscience, 13, 453, doi: 10.1038/s41561-020-0578-1

Lichtenberg, T., & Miguel, Y. 2025, in Treatise on Geochemistry (Third edition), third edition edn., ed. A. Anbar & D. Weis (Oxford: Elsevier), 51–112, doi: https://doi.org/10.1016/B978-0-323-99762-1.00122-4

Lim, O., Benneke, B., Doyon, R., et al. 2023, The Astrophysical Journal Letters, 955, L22, doi: 10.3847/2041-8213/acf7c4

Lincowski, A. P., Meadows, V. S., Zieba, S., et al. 2023, The Astrophysical Journal Letters, 955, L7, doi: 10.3847/2041-8213/acee02

Lodders, K. 2003, The Astrophysical Journal, 591, 1220, doi: 10.1086/375492

Luger, R., Sestovic, M., Kruse, E., et al. 2017, Nature Astronomy, 1, 1, doi: 10.1038/s41550-017-0129

Luo, H., Dorn, C., & Deng, J. 2024, Nature Astronomy, 8, doi: 10.1038/s41550-024-02347-z

Luo, Y., Xiang, S., Li, J., et al. 2023, Physical Review B, 107, 134116, doi: 10.1103/PhysRevB.107.134116

Luque, R., & Pallé, E. 2022, Science, 377, 1211, doi: 10.1126/science.abl7164

Léger, A., Selsis, F., Sotin, C., et al. 2004, Icarus, 169, 499, doi: https://doi.org/10.1016/j.icarus.2004.01.001

Melosh, H. 2007, Meteoritics & planetary science, 42, 2079

Miozzi, F., Matas, J., Guignot, N., et al. 2020, Minerals, 10, 100, doi: 10.3390/min10020100

Musella, R., Mazevet, S., & Guyot, F. 2019, Physical Review B, 99, 064110, doi: 10.1103/PhysRevB.99.064110

Nixon, M. C., Somers, R. S., Savel, A. B., et al. 2025, https://arxiv.org/abs/2510.07367

Noack, L., & Lasbleis, M. 2020, Astronomy & Astrophysics, 638, A129, doi: 10.1051/0004-6361/202037723

Pass, E. K., Charbonneau, D., & Vanderburg, A. 2025, The Astrophysical Journal Letters, 986, L3

Piaulet-Ghorayeb, C., Benneke, B., Turbet, M., et al. 2025, The Astrophysical Journal, 989, 0, doi: 10.3847/1538-4357/adf207

Quarles, B., Quintana, E. V., Lopez, E., Schlieder, J. E., & Barclay, T. 2017, The Astrophysical Journal Letters, 842, L5, doi: 10.3847/2041-8213/aa74bf

Radica, M., Piaulet-Ghorayeb, C., Taylor, J., et al. 2025, The Astrophysical Journal Letters, 979, L5, doi: 10.3847/2041-8213/ada381

Schaefer, L., & Fegley, B. 2017, The Astrophysical Journal, 843, 120, doi: 10.3847/1538-4357/aa784f

Schlichting, H. E., & Young, E. D. 2022, The Planetary Science Journal, 3, 127, doi: 10.3847/PSJ/ac68e6

Schoonenberg, D., Liu, B., Ormel, C. W., & Dorn, C. 2019, Astronomy and Astrophysics, 627, 1, doi: 10.1051/0004-6361/201935607

Seager, S., Kuchner, M., Hier-Majumder, C. A., & Militzer, B. 2007, The Astrophysical Journal, 669, 1279, doi: 10.1086/521346

Seo, C., Ito, Y., & Fujii, Y. 2024, The Astrophysical Journal, 975, 14, doi: 10.3847/1538-4357/ad7461

Siebert, J., Badro, J., Antonangeli, D., & Ryerson, F. J. 2012, Earth and Planetary Science Letters, 321-322, 189, doi: 10.1016/j.epsl.2012.01.013

Siebert, J., Badro, J., Antonangeli, D., & Ryerson, F. J. 2013, Science, 339, 1194, doi: 10.1126/science.1227923

Spaargaren, R. J., Wang, H. S., Mojzsis, S. J., Ballmer, M. D., & Tackley, P. J. 2023, The Astrophysical Journal, 948, 53, doi: 10.3847/1538-4357/acac7d

Stewart, S. T., Davies, E. J., Duncan, M. S., et al. 2020, in 21st Biennial APS Conference on Shock Compression of Condensed Matter, 080003, doi: 10.1063/12.0000946

Stixrude, L. 2014, Philosophical Transactions of the Royal Society A: Mathematical, Physical and Engineering Sciences, 372, 20130076, doi: 10.1098/rsta.2013.0076

Stixrude, L., & Lithgow-Bertelloni, C. 2022, Geophysical Journal International, 228, 1119, doi: 10.1093/gji/ggab394

Trønnes, R., Baron, M., Eigenmann, K., et al. 2019, Tectonophysics, 760, 165, doi: https://doi.org/10.1016/j.tecto.2018.10.021

Unterborn, C. T., Desch, S. J., Hinkel, N. R., & Lorenzo, A. 2018a, Nature Astronomy, 2, 297, doi: 10.1038/s41550-018-0411-6

Unterborn, C. T., Desch, S. J., Hinkel, N. R., & Lorenzo Jr, A. 2018b, arXiv. http://arxiv.org/abs/1706.02689

Valencia, D., Sasselov, D. D., & O'Connell, R. J. 2007, The Astrophysical Journal, 665, 1413, doi: 10.1086/519554

Van Looveren, G., Saikia, S. B., Herbort, O., et al. 2025, Astronomy & Astrophysics, 694, A310

Wang, H. S., Lineweaver, C. H., & Ireland, T. R. 2018, Icarus, 299, 460, doi: 10.1016/j.icarus.2017.08.024

Werlen, A., Dorn, C., Schlichting, H. E., Grimm, S. L., & Young, E. D. 2025, The Astrophysical Journal Letters, 988, L55, doi: 10.3847/2041-8213/adf185

Young, E. D., Werlen, A., Marcum, S. P., Stixrude, L., & Dullemond, C. P. 2025, https://arxiv.org/abs/2507.00947

Zeng, L., Jacobsen, S. B., Sasselov, D. D., et al. 2019, Proceedings of the National Academy of Sciences of the United States of America, 116, 9723, doi: 10.1073/pnas.1812905116

Zieba, S., Kreidberg, L., Ducrot, E., et al. 2023, Nature, 620, 746, doi: 10.1038/s41586-023-06232-z